Mechanical Systems and Signal Processing 184 (2023) 109720

Contents lists available at ScienceDirect

Mechanical Systems and Signal Processing

journal homepage: www.elsevier.com/locate/ymssp

A Gaussian process regression reduced order model for geometrically nonlinear structures

Kyusic Park [a,*], Matthew S. Allen [b]

[a] University of Wisconsin Madison, Department of Mechanical Engineering, Madison, WI, 53705, United States
[b] Brigham Young University, Department of Mechanical Engineering, Provo, UT, 84602, United States

ARTICLE INFO

Communicated by J.E. Mottershead

Keywords:
Nonlinear dynamics
Geometric nonlinearity
Reduced order modeling
Data-driven modeling
Model uncertainty
Gaussian process regression

ABSTRACT

Reduced order models, such as Hollkamp and Gordon's Implicit Condensation and Expansion (ICE) model, are a highly efficient alternative to full-order finite element models (FEM) of geometrically nonlinear structures. However, a reduced order model (ROM) is typically only valid for one FEM. It does not capture how each ROM coefficient changes due to variations in the FEM (e.g., design parameters or uncertainties), so if the FEM is updated then the ROM needs to be re-computed with a new set of static load–displacement data. This study presents a data-driven reduced order modeling approach that creates a single ROM that incorporates design variations in FEM. The proposed method applies Gaussian Process Regression (GPR) to the ICE approach, making each coefficient in an ICE ROM a regression model with respect to a collection of FEMs with varying material properties or geometric parameters. Once the GPR ROM has been identified, one can immediately produce an ICE ROM for a set of FEM parameters without a need to solve any static load–displacement cases on the full FEM. This dramatically enhances the computational efficiency and could be helpful when model uncertainty needs to be considered or when seeking to update a model to correlate with measurements. Additionally, the coefficients of a ROM can often change considerably if the scale on the load–displacement data changes, so it can be difficult to know whether the scaling that was chosen has really identified an accurate ROM. The proposed GPR ROM estimates the mean ROM coefficients for a range of load scaling as well as the uncertainty on each ROM coefficient with respect to the load level. This can be used to gauge the success of the ROM identification and to eliminate ROM coefficients that are unimportant and hence highly variable. The proposed GPR ROM approach is evaluated by applying it to flat and curved beam structures, revealing that the advantages outlined above can be realized with a relatively modest increase in cost relative to a traditional ICE ROM.

1. Introduction

Thin panels of high-speed vehicles exhibit highly complex behaviors when subjected to severe aerodynamic or aerothermal stress [1,2]. Under such conditions, any large deformation of the thin structures induces a significant change of stiffness, and the structures may eventually lose stability to flutter [3,4] or buckle [5,6]. The finite element (FE) method has been well-established over the past decades, and FE models (FEMs) have functioned as digital twins of geometrically nonlinear panels to simulate complex behaviors in various types of dynamic responses, such as time history response, frequency response functions (FRFs), power spectral

* Corresponding author.
E-mail address: kpark93@wisc.edu (K. Park).

https://doi.org/10.1016/j.ymssp.2022.109720
Received 10 January 2022; Received in revised form 23 July 2022; Accepted 21 August 2022
Available online 5 September 2022

densities (PSDs) and nonlinear normal modes (NNMs). Although the FE method provides accurate predictions, the computational cost of integrating the nonlinear response becomes prohibitive as FEMs become large, yet many degrees of freedom may be needed to capture the geometric complexity of modern aircraft panels [7,8]. The computational overhead becomes even more critical if one needs to update a FEM to better reproduce a measured response, as this requires simulating the model iteratively after making changes to the FEM parameters [9–11].

A reduced order model (ROM) is a simplification of a FEM that alleviates the computational burden. In reduced order modeling, one typically projects the full-order equations of motion onto a modal subspace by the Galerkin method, greatly reducing the number of variables that must be time-integrated to find the dynamic response. The reduced modal equations are typically obtained by a non-intrusive approach, where a commercial FE solver is used to obtain several nonlinear static solutions, in which the structure is subjected to loads or displacements in the shapes of the basis vectors [12,13]. Displacement based approaches, such as Equivalent Linearization Using a Stiffness Evaluation Procedure (ELSTEP) in [14] and the Enforced Displacement method (ED) in [15], apply a set of static displacements in the shape of few dominant modes to solve for the corresponding reaction forces, and project the displacement–force sets onto the reduced modal coordinates to compute the nonlinear stiffness coefficients of the ROM. Using the force based approach, on the other hand, one applies a prescribed set of static forces and solves for the resulting displacement [16,17]. Hollkamp et al. [18] revealed that the force based approach has some distinct advantages, in that the nonlinear responses can often be captured using only a few dominant bending modes as basis vectors, because it implicitly captures the membrane motions; they named the corresponding approach implicit condensation (IC). They further extended this approach by adding the ability to recover the membrane displacements in a post-processing step, using a method that is called implicit condensation and expansion (ICE) [19]. In either case it can be far more efficient than traditional Galerkin projection or proper orthogonal decomposition (POD), because the membrane displacements are captured implicitly and so they do not need to be included in the reduction basis. While ELSTEP and ICE are the two most common non-intrusive reduced order modeling techniques, many others have been developed recently that take a different view. For example, the spectral submanifold approaches [20,21] and the quadratic manifold approach [22]. For more detail the reader is referred to the recent review by Touze et al. [23].

While reduced order modeling methods have been shown to provide accurate dynamic simulations with dramatically reduced computational cost, some important challenges still exist. First, a typical ROM can only represent a single FEM configuration and does not account for the variations in FEM. If anything in the FEM changes, one must recompute the corresponding ROM with a new set of static load–displacement solutions. This can make ROM-based simulation repetitive and tedious as one frequently does need to repeat the simulations after changing the FEM slightly, in order to study manufacturing variability or model uncertainty. Second, the number of nonlinear terms in a ROM increases with the fourth power of the number of modes, but not every term contributes equally to capturing the nonlinear responses. For example, Shen et al. [24] recently demonstrated that the resonant terms in an ICE ROM have a stronger influence on the dynamics than the remaining nonlinear terms. It would be desirable to be able to identify only those terms that are most important when creating the ROM. Lastly, in spite of considerable research on the topic, manual intervention and expertise are still needed to obtain a valid ROM for a given FEM. One reason for this is the fact that some of the ROM coefficients tend to be sensitive to the static load cases that are used to identify the ROM [15,25]. As a result, it becomes difficult to use a ROM for nonlinear model updating because manual intervention is needed at each step and small inaccuracies from one ROM to the next can corrupt the process [26–28].

The present study proposes a new data-driven reduced order modeling approach for geometrically nonlinear structures that addresses these challenges. The proposed approach takes advantage of the ICE form of the ROM, which is known to be efficient and accurate for capturing geometric nonlinearity, the physics of interest. However, whereas each polynomial coefficient in an ICE ROM is constant, in the approach proposed here each coefficient is a function of the parameters of the FEM, and the ROM is trained with data from a collection of FEMs where the parameters of interest are allowed to vary. As a result, once the training is complete one can immediately generate a ROM for any set of FEM parameters within the range of the training data, without computing any additional static load cases. Furthermore, the gradient of the ROM with respect to the FEM parameters is embedded in the ROM, and this could be useful for model updating.

Specifically, this work proposes to use a Gaussian Process Regression (GPR) to model the polynomial coefficients in the ICE ROM. GPR has been acknowledged as a powerful regression tool due to its Bayesian approach [29,30]. The GPR method specifies a regression model by its mean and covariance functions and so is non-parametric and flexible for both simple and complex problems. One of the strengths of the Gaussian process (GP) model is that it quantifies the predictive uncertainty of the model with respect to the input variables. In our approach, the GP model is trained using the FEM–ICE ROM (input–output) training sets to formulate a Gaussian prior for each ROM parameter (i.e., each of the linear and nonlinear coefficients of the ICE ROM). Then, using the trained GP model of the ROM (hereafter termed a GPR ROM) one can quickly estimate the posterior mean and variance of any term in the ROM for any set of FEM parameters within the range of the training data. Furthermore, we randomize the load cases that are used for computing the training data so that the trained GPR ROM can also quantify the uncertainty of the ROM coefficients with respect to the applied loads. This provides a means to identify the inconsistent and sensitive ROM coefficients with respect to the load cases, and eventually to filter out the redundant terms, significantly reducing the size of the ROM.

Several other researchers have explored related data-driven reduced order modeling methods for various nonlinear systems. Hesthaven et al. demonstrated a non-intrusive regression ROM for nonlinear structural or time-dependent problems, which projects the high-fidelity solutions of discrete FEM sets onto a reduced space [31–34]. On that reduced space their ROM was composed of an artificial neural network (ANN) and Gaussian Process Regression (GPR) models. Note that in their studies, they directly projected a set of full-order dynamic responses onto a reduced space using the proper orthogonal decomposition (POD) method, and used that relatively expensive data to train the model. They reported that their data-driven ROMs could quickly evaluate the

reduced-order responses from the regression map without a need of computing the full order responses. Data-driven ROMs have further been studied particularly for computational fluid dynamics, in which Hasagawa et al. [35] applied the convolutional neural network autoencoder (CNN-AE) to map a high-dimensional unsteady flow to a reduced latent space. Ma et al. [36] recently applied GPR to dynamic systems with moving boundaries such as fluid–solid interactions, and inferred the time-evolution of the temporal coefficients and the parameters characterizing the moving boundary in a reduced space. While there are several similarities and many of the preceding studies have employed GPR, none has coupled GPR with the ICE ROM as is proposed here.

One common theme in those works is that, to be successful, the chosen ROM scheme must be able to accurately capture the underlying physics with a minimal set of parameters, to minimize the training data needed. The ICE ROM proposed here is highly efficient in that regard. Furthermore, the cited data-driven ROM studies train the ROM using a set of full-order dynamic responses, whereas the ICE methodology generates a set of training data that is far more rich than a dynamic response by using a set of quasi-static loads in the shape of the eigenvectors of interest. This makes the offline ROM training stage more computationally efficient and robust. Furthermore, the ICE ROM form is versatile and can be readily applied to simulate the response using time integration or to compute the FRFs, PSDs and/or NNMs [15].

The paper is organized as follows. Section 2 outlines the underlying theory of the proposed data-driven ROM and its algorithm based on Gaussian process regression. In Section 3, the method is evaluated by applying it to two geometrically nonlinear structures. The conclusion and future works are discussed in Section 4.

2. Theoretical development

2.1. Reduced order modeling of geometrically nonlinear structure

The n-DOF FE equations of motion for a geometrically nonlinear structure can be written as

$$\mathbf{M}(\mathbf{p})\ddot{\mathbf{x}} + \mathbf{C}(\mathbf{p})\dot{\mathbf{x}} + \mathbf{K}(\mathbf{p})\mathbf{x} + \mathbf{f}_{\text{nl}}(\mathbf{x},\mathbf{p}) = \mathbf{f}(t) \tag{1}$$

where $\mathbf{p} \in \mathbb{R}^d$ is the d-dimensional parameter set that characterizes any uncertain parameters in the FEM, such as material properties, uncertain dimensions, and boundary condition stiffness. $\mathbf{M}$, $\mathbf{C}$, and $\mathbf{K}$ are the corresponding $n \times n$ mass, damping, and linear stiffness matrices. $\mathbf{f}_{\text{nl}}$ denotes the $n \times 1$ nonlinear restoring force that captures the nonlinearity of the system with respect to the displacements $\mathbf{x}$, and $\mathbf{f}(t)$ is the $n \times 1$ external force. The full FE equations of motion in the physical domain can be projected to a modal subspace by solving an eigenvalue problem:

$$(\mathbf{K}(\mathbf{p}) - {\omega_r}^2(\mathbf{p})\mathbf{M}(\mathbf{p}))\boldsymbol{\Phi}_r(\mathbf{p}) = 0 \tag{2}$$

where ω_r is the rth linear natural frequency and $\boldsymbol{\Phi}_r$ is its $n \times 1$ mass normalized mode shape. The full-order nonlinear response can be approximated by a linear combination of m modal coordinates as

$$\mathbf{x}(t) = \boldsymbol{\Phi}(\mathbf{p})\mathbf{q}(t) \tag{3}$$

where $\boldsymbol{\Phi}$ is the n x m mass normalized mode shape matrix, and $\mathbf{q}$ is the m x 1 vector of modal coordinates.

The nonlinear reduced order model (ROM) aims to approximate the full-order nonlinear equations with a dramatically reduced set of dominant modal equations ($n \gg m$). The rth nonlinear modal equation can be derived by substituting Eq. (3) into Eq. (1) and pre-multiplying by $\boldsymbol{\Phi}^{\text{T}}$:

$$\ddot{q}_r + c_r(\mathbf{p})\dot{q}_r + \omega_r^2(\mathbf{p})q_r + \theta_r(q_1, q_2, \ldots, q_m, \mathbf{p}) = \boldsymbol{\Phi}_r(\mathbf{p})^{\text{T}}\mathbf{f}(t) \tag{4}$$

where θ_r is the modal nonlinear restoring force. When the FEM is geometrically nonlinear and linear elastic, the nonlinear restoring force θ_r can be well approximated by a cubic polynomial [37,38], which can be written as

$$\theta_r(q_1, q_2, \ldots, q_m, \mathbf{p}) = \sum_{i=1}^{m}\sum_{j=i}^{m}\alpha_r(i,j,\mathbf{p})q_i q_j + \sum_{i=1}^{m}\sum_{j=i}^{m}\sum_{k=j}^{m}\beta_r(i,j,k,\mathbf{p})q_i q_j q_k \tag{5}$$

where α_r and β_r are the quadratic and cubic nonlinear stiffness terms. The number of nonlinear terms in a ROM is defined as $N_{\text{nl}} = m\left(m + m^2 + \frac{m!}{2!(m-2)!} + \frac{m!}{3!(m-3)!}\right)$, indicating that the number increases with the fourth power of the number of modes used in the reduced basis. When no damping is considered, the ROM coefficient matrix, which contains both linear and nonlinear coefficients of the ROM can be defined as

$$\mathbf{Y} = \begin{bmatrix} \omega_1 & \alpha_1(1,1) & \alpha_1(1,2) & \cdots & \alpha_1(m,m) & \beta_1(1,1,1) & \beta_1(1,1,2) & \cdots & \beta_1(m,m,m) \\ \omega_2 & \alpha_2(1,1) & \alpha_2(1,2) & \cdots & \alpha_2(m,m) & \beta_2(1,1,1) & \beta_2(1,1,2) & \cdots & \beta_2(m,m,m) \\ & & & \cdots & & & & \cdots & \\ \omega_m & \alpha_m(1,1) & \alpha_m(1,2) & \cdots & \alpha_m(m,m) & \beta_m(1,1,1) & \beta_m(1,1,2) & \cdots & \beta_m(m,m,m) \end{bmatrix} \tag{6}$$

Note that the ROM coefficients should obey certain symmetries, for example, $\beta_i(i,i,j) = 3\beta_j(i,i,i)$, as explained in [16,19]. However, to enforce these symmetries, all of the coefficients must be found in a single least-squares problem and this might increase numerical ill-conditioning. In this work, those symmetries were not enforced (i.e., we used Hollkamp's "unconstrained" approach to find the coefficients), as this was found by Kuether et al. [15] to produce more reliable ROMs.

2.2. Applied loads procedure for reduced order modeling

Non-intrusive methods for reduced order modeling postulate the form given in Eqs (4)–(5) and use a set of static load–displacement data to identify the coefficients α_r and β_r [12]. This work uses the applied loads procedure (referred as ICE) introduced by Hollkamp & Gordon [19] to estimate the nonlinear coefficients.

Accordingly, a set of static forces are applied to the full-order FEM, each of which is designed to excite only the modes in the reduced basis:

$$\mathbf{F}_p = \mathbf{M}(\boldsymbol{\Phi}_1 c_1 + \boldsymbol{\Phi}_2 c_2 + \cdots + \boldsymbol{\Phi}_m c_m) \tag{7}$$

where $\mathbf{F}_p$ is the prescribed multi-mode static force and c_r is the rth modal forcing coefficient. The scalar c_r controls the degree of geometric nonlinearity that $\mathbf{F}_p$ imposes on the system, and can be further defined as

$$c_r = \frac{f_r}{\boldsymbol{\Phi}_{r,\max}}\omega_r^2 \tag{8}$$

where $\boldsymbol{\Phi}_{r,\max}$ is the mode shape of the rth mode at the point where the deformation is maximum and f_r is the force scaling factor of the rth mode. f_r can be interpreted as the maximum displacement that the static force $\mathbf{F}_p$ would cause for the linearized system. Kuether et al. in [15] have recently shown that f_r on the order of the thickness typically allows a ROM to sufficiently capture the geometric nonlinearity of thin, flat structures. They also demonstrated that a ROM is sensitive to the force scaling factor and empirical trials are required to find an f_r that produces an accurate ROM.

The nonlinear coefficients α_r and β_r of rth modal equation in Eq. (5), can be identified by solving a least-squares problem. These nonlinear coefficients then populate from second to last element of the rth row of the ROM coefficient matrix $\mathbf{Y}$ in Eq. (6). The least-squares problem uses a number of forces $\mathbf{F}_p$ with different combinations of terms in Eq. (7) and the resulting sets of static responses $\mathbf{x}_p$. The static responses can then be projected onto the modal coordinate as $q_r = \boldsymbol{\Phi}_r^{\mathrm{T}}\mathbf{M}\mathbf{x}_p$, and used to formulate the least-squares problem for the rth mode, which can be written as

$$\mathbf{Q}\boldsymbol{\Theta}_r = \mathbf{G}_r \tag{9}$$

where $\boldsymbol{\Theta}_r$ is the $\frac{N_{\mathrm{nl}}}{m} \times 1$ nonlinear stiffness coefficient vector, (i.e., $\boldsymbol{\Theta}_r = [\boldsymbol{\alpha}_r, \boldsymbol{\beta}_r]^{\mathrm{T}}$), $\mathbf{Q}$ is the $N_p \times \frac{N_{\mathrm{nl}}}{m}$ polynomial combinations of the modal responses $q_1, q_2, \ldots, q_m$, and $\mathbf{G}_r$ is the $N_p \times 1$ nonlinear internal force vector:

$$\mathbf{Q} = \begin{bmatrix} q_1^2[1] & q_1q_2[1] & \cdots & q_m^2[1] & q_1^3[1] & q_1^2q_2[1] & \cdots & q_m^3[1] \\ q_1^2[2] & q_1q_2[2] & \cdots & q_m^2[2] & q_1^3[2] & q_1^2q_2[2] & \cdots & q_m^3[2] \\ & & \cdots & & & & \cdots & \\ q_1^2[N_p] & q_1q_2[N_p] & \cdots & q_m^2[N_p] & q_1^3[N_p] & q_1^2q_2[N_p] & \cdots & q_m^3[N_p] \end{bmatrix} \tag{10}$$

$$\mathbf{G}_r = \begin{bmatrix} \boldsymbol{\Phi}_r^{\mathrm{T}}\mathbf{F}_p[1] - \omega_r^2 q_r[1] \\ \boldsymbol{\Phi}_r^{\mathrm{T}}\mathbf{F}_p[2] - \omega_r^2 q_r[2] \\ \vdots \\ \boldsymbol{\Phi}_r^{\mathrm{T}}\mathbf{F}_p[N_p] - \omega_r^2 q_r[N_p] \end{bmatrix} \tag{11}$$

Then, the nonlinear stiffness coefficients vector $\boldsymbol{\Theta}_r$ can be computed using the closed form of the least-squares solution, i.e.,

$$\boldsymbol{\Theta}_r = (\mathbf{Q}^{\mathrm{T}}\mathbf{Q})^{-1}\mathbf{Q}^{\mathrm{T}}\mathbf{G}_r \tag{12}$$

To solve this equation one must have $N_p \geq \frac{N_{\mathrm{nl}}}{m}$. Solving this equation for $\boldsymbol{\Theta}_r$ provides the rth row of $\mathbf{Y}$ in Eq. (6) and is repeated for each mode $r = 1, \ldots, m$ to compute the full set of ROM coefficients.

2.3. Proposed Gaussian Process Regression Reduced Order Model (GPR ROM)

This section presents the proposed GPR ROM, which relies on the form of the ICE ROM introduced in the previous sections. A Gaussian process (GP) model specifies any finite collection of random variables by its mean and covariance function based on the assumption that the collection obeys a joint Gaussian distribution [29]. In our approach, a collection of N_{tr} input FEMs is created, each with a different realization of the parameter vector, $\mathbf{p}$. The parameter vectors can be collected into a matrix, $\mathbf{P}_{\mathrm{tr}} = [\mathbf{p}_1, \mathbf{p}_2, \ldots, \mathbf{p}_{N_{\mathrm{tr}}}]^{\mathrm{T}} \in \mathbb{R}^{N_{\mathrm{tr}} \times d}$ and each FEM is used to estimate the corresponding set of ICE ROM coefficients, which are also collected into an array $\mathbf{Y}_{\mathrm{tr}} = [\mathbf{Y}_1, \mathbf{Y}_2, \ldots, \mathbf{Y}_{N_{\mathrm{tr}}}]^{\mathrm{T}}$. This is a 3D array of size $N_{\mathrm{tr}} \times m \times (\frac{N_{\mathrm{nl}}}{m} + 1)$ where the ith matrix, defined in Eq. (6), is denoted $\mathbf{Y}_i$.

Let y denote the (j,k)th term in the ith ROM coefficient matrix $\mathbf{Y}_i$, corresponding to a single term in the ROM. Then, each ROM coefficient y can be described by a GP model, which will depend on the FEM parameters $\mathbf{p}$. The GP model can be identified using the known FEM parameters $\mathbf{P}_{\mathrm{tr}}$ and the ROM coefficients estimated from each of the training FEMs using the ICE method $\mathbf{y}_{\mathrm{tr}} = [y_1, y_2, \ldots, y_{N_{\mathrm{tr}}}]^{\mathrm{T}}$.

Based on the assumption that the collection of y obeys the joint Gaussian distribution, the GP function ψ describing ROM coefficient y can be written as

$$\psi(\mathbf{p}) \sim \mathcal{GP}(\eta, \kappa) \tag{13}$$

where $\mathcal{GP}$ denotes that the function ψ is distributed as a Gaussian Process, and η and κ are the mean and covariance functions that describe the ROM coefficient distribution. In this study, the mean function is defined with a constant, $\eta = \eta_m$, and the covariance function κ is defined with the automatic relevance determination squared exponential (ARD SE) kernel [39]:

$$\kappa(\mathbf{p}_i, \mathbf{p}_j) = \sigma_f^2 \exp\left(-\frac{1}{2}\sum_{k=1}^{d}\frac{(p_{i,k} - p_{j,k})^2}{l_k^2}\right) \tag{14}$$

where $p_{i,k}$ is the kth parameter, or the kth element of $\mathbf{p}_i$, σ_f is the output standard deviation, and l_k is the kth individual length scale. Note that the covariance is a function of the distance between the corresponding FEM parameter vectors $\mathbf{p}_i$. Based on the assumption that the observed ROM coefficient set $\mathbf{y}_{\text{tr}}$ is corrupted by an independent noise term ϵ_n, the ROM coefficient y can be expressed as the following GP model:

$$y(\mathbf{p}) = \psi(\mathbf{p}) + \epsilon_n, \quad \epsilon_n \sim \mathcal{N}(0, {\sigma_n}^2) \tag{15}$$

where ${\sigma_n}^2$ is the noise variance. The GP model in Eq. (15) can be trained by optimizing the hyperparameters $\boldsymbol{\theta}_h$ in its mean and covariance functions, e.g., $\boldsymbol{\theta}_h = \{\eta_m, \sigma_f, l_1, l_2, \ldots, l_d, \sigma_n\}$. This is achieved by estimating the maximum likelihood of the GP model with respect to the training sets [29], which can be expressed as

$$\boldsymbol{\theta}_h = \underset{\boldsymbol{\theta}_h}{\text{argmax}} \log p(\mathbf{y}_{\text{tr}}|\mathbf{P}_{\text{tr}}) = \underset{\boldsymbol{\theta}_h}{\text{argmax}}\left(-\frac{1}{2}\log|\boldsymbol{\Sigma}(\boldsymbol{\theta}_h)| - \frac{1}{2}(\mathbf{y}_{\text{tr}} - \boldsymbol{\mu}(\boldsymbol{\theta}_h))^{\text{T}}\boldsymbol{\Sigma}^{-1}(\boldsymbol{\theta}_h)(\mathbf{y}_{\text{tr}} - \boldsymbol{\mu}(\boldsymbol{\theta}_h)) - \frac{N_{\text{tr}}}{2}\log(2\pi)\right) \tag{16}$$

where $\boldsymbol{\mu}(\boldsymbol{\theta}_h)$ is the $N_{\text{tr}} \times 1$ mean vector estimated by the mean function hyperparameter, i.e., $\mu_i(\boldsymbol{\theta}_h) = \eta_m$, and $\boldsymbol{\Sigma}(\boldsymbol{\theta}_h)$ is the $N_{\text{tr}} \times N_{\text{tr}}$ covariance matrix estimated by the covariance function hyperparameters in Eq. (14) and the noise function hyperparameter σ_n, i.e., $\Sigma_{ij}(\boldsymbol{\theta}_h) = \kappa(\mathbf{p}_i, \mathbf{p}_j) + \sigma_n^2\delta_{ij}$ (where $\delta_{ij} = 1$ iff $i = j$ is the Kronecker delta).

The distribution of the training sets $\mathbf{y}_{\text{tr}}$ can be used as a prior from a Bayesian perspective, and the posterior distribution for a new test set $\mathbf{y}_*$ can be estimated based on the conditional distribution of joint Gaussian variables [29], which can be written as

$$\mathbf{y}_*|\mathbf{P}_*, \mathbf{P}_{\text{tr}}, \mathbf{y}_{\text{tr}} \sim \mathcal{N}(\boldsymbol{\mu}_* + \boldsymbol{\Sigma}_*^{\text{T}}\boldsymbol{\Sigma}^{-1}(\mathbf{y}_{\text{tr}} - \boldsymbol{\mu}),\ \boldsymbol{\Sigma}_{**} - \boldsymbol{\Sigma}_*^{\text{T}}\boldsymbol{\Sigma}^{-1}\boldsymbol{\Sigma}_*), \tag{17}$$

where $\boldsymbol{\mu}_*$ is the mean of the new test set, which is identical to $\boldsymbol{\mu}$ (as the mean in this work is defined with a constant). $\boldsymbol{\Sigma}_*$ is the training-test set covariance $\kappa(\mathbf{P}_{\text{tr}}, \mathbf{P}_*)$ and $\boldsymbol{\Sigma}_{**}$ is the test set covariance $\kappa(\mathbf{P}_*, \mathbf{P}_*)$. The mean and variance of the ROM coefficient can thus be easily estimated for any given set of FEM parameters.

In this work the proposed GPR ROM framework was implemented in MATLAB® using the built-in function *fitrgp*.

2.4. Proposed GPR ROM training framework

As mentioned in Section 2.2, many of the coefficients in a typical ICE ROM may be highly variable with respect to the static load cases used to estimate them, and hence they do not contribute significantly to the set of static load displacement data. The GPR ROM quantifies the predictive uncertainty in each coefficient, and this is utilized here to detect those ICE ROM coefficients that are not important in fitting the training data. The first term on the right in Eq. (17) provides a prediction of an ICE ROM for any FEM parameter vector $\mathbf{p}_*$ (or set of parameter vectors $\mathbf{P}_*$) that is within the bounds of the training data. The second term in Eq. (17) provides information about the predictive variance in each ROM coefficient over the range of training data. This section describes how this functionality is employed to filter out uncertain or redundant nonlinear coefficients, in order to keep the ROM as small as possible.

There are several important reasons for filtering out the unnecessary ROM coefficients. Erroneous ROM coefficients can produce inaccurate dynamic responses, or even cause the time integration algorithm to fail, as shown in Kuether's work [15]. Hence, a ROM that excludes those coefficients is likely to be more robust when running the dynamic simulations. The ROM is also smaller and hence less expensive to evaluate and this can speed up dynamic simulations. It becomes even more compelling to minimize the number of ROM coefficients when one wishes to update a ROM to correlate with experimental measurements. For example, in some recent studies [26–28], the nonlinear coefficients were used as design variables and were adjusted until the dynamic responses of the ROM matched those from measurements. This process becomes much more difficult as the number of ROM coefficients, and hence the number of design variables, increases. In this regard the filtering capability of the proposed GPR ROM method could be extremely valuable. Of course, if the size of the ROM was not a concern in the application of interest, one could skip the procedure outlined in this section and use the GPR ROM as identified and simply recognize that the ROM coefficients that were more variable might be less accurate.

The proposed procedure for training and reducing the size of a GPR ROM is outlined in Fig. 1. The FEM parameters are sampled within the prescribed range $[\mathbf{p}_{\min}, \mathbf{p}_{\max}]$ to create N_{tr} sets, captured in the vectors $\mathbf{p}_i$ that comprise a matrix $\mathbf{P}_{\text{tr}} = [\mathbf{p}_1, \mathbf{p}_2, \ldots, \mathbf{p}_{N_{\text{tr}}}]^{\text{T}}$. Each of those is used to create a set of N_p randomized static loads, for a total of N_{tr} sets of N_p loads each. Each set of N_p loads provides a set of data $\mathbf{D}_i = [\mathbf{Q}, \mathbf{G}_1, \ldots, \mathbf{G}_{\mathbf{m}}]$ as defined in Eqs. (10)–(11). The total set of data ($[\mathbf{D}_1, \mathbf{D}_2, \ldots, \mathbf{D}_{N_{\text{tr}}}]$) is denoted $\mathbf{D}_{tr}$.

In the next step a boolean matrix $\mathbf{B}_{\text{nl}}$ is defined to select which ROM coefficients, among the entire set of possible coefficients, are identified in each step. Specifically, $\mathbf{B}_{\text{nl}}$ is a $m \times \frac{N_{\text{nl}}}{m}$ matrix, whose rth row $\mathbf{B}_{\text{nl},r}$ has ones in the locations of the columns of $\mathbf{Q}$ and the rows of $\boldsymbol{\Theta}_r$ to retain in Eq. (12) and zeros elsewhere. Initially $\mathbf{B}_{\text{nl},r}$ is a vector of ones, indicating that all coefficients are sought in the first step. Then, elements become zeros in subsequent steps corresponding to the coefficients that are no longer desired. In each step, an equation identical to Eq. (12) is solved, but with the unneeded rows of $\boldsymbol{\Theta}_r$ and columns of $\mathbf{Q}$ removed, to

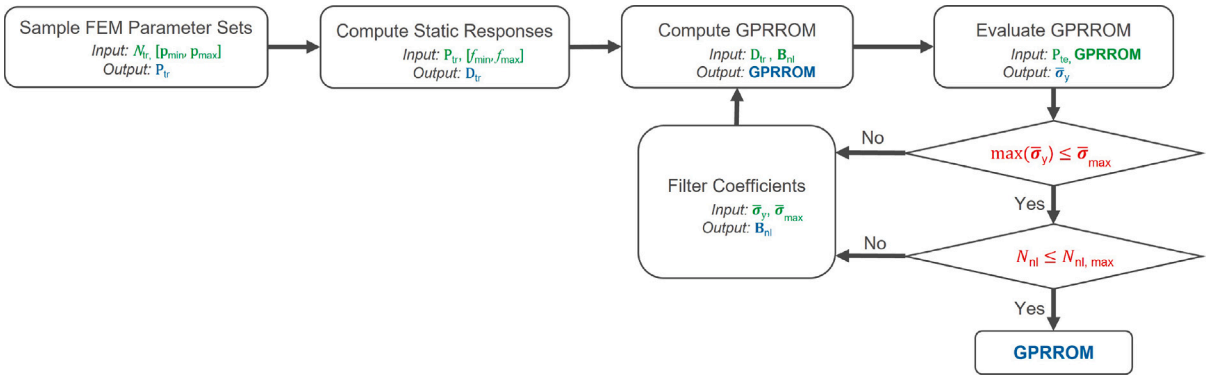

Fig. 1. Illustration of GPR ROM training framework. ($\mathbf{B}_{\text{nl}}$ is the boolean matrix of the filtered nonlinear coefficients in the GPR ROM.)

obtain an estimate for the desired ROM coefficients $\boldsymbol{\Theta}_r$. This data is obtained for each of the trials $i = 1, \ldots, N_{\text{tr}}$ and used to create a GPR model for the ROM coefficients as in Eq. (15).

Once a GPR ROM has been identified for a particular parameter set, the predictive variance of each ROM coefficient, $\sigma^2_{\text{y},i}$ is simply the ith diagonal component of the conditional covariance in Eq. (17). In order to quantify the predictive variance over the full range of the FEM parameters, the GPR ROM is evaluated at a collection of N_{te} sets of FEM parameters $\mathbf{P}_{\text{te}} = [\mathbf{p}_1, \mathbf{p}_2, \ldots, \mathbf{p}_{N_{\text{te}}}]^{\text{T}}$ within the prescribed parameter range. Then the average predictive standard deviation (STD) of each ROM coefficient is defined as follows

$$\bar{\sigma}_{\text{y}} = \frac{1}{N_{\text{te}}} \sum_{i=1}^{N_{\text{te}}} \sigma_{\text{y},i} \tag{18}$$

Any ROM coefficient with $\bar{\sigma}_{\text{y}}$ greater than a pre-defined maximum allowable STD ($\bar{\sigma}_{\max}$) can be removed from the GPR ROM. Those coefficients have exhibited a high variance over the training data, and hence are very sensitive to the load scaling.

In the method used in this paper, a limit was placed on the maximum allowable size of the GPR ROM ($N_{\text{nl, max}}$), based on the presumption that a large ROM has a number of redundant coefficients. When the number of nonlinear coefficients kept in the GPR ROM exceeds this bound, i.e., $N_{\text{nl}} > N_{\text{nl, max}}$, then at least one nonlinear coefficient having the largest $\bar{\sigma}_y$ is filtered out. The process continues as outlined in Fig. 1 until a GPR ROM of the desired size is obtained.

The computational cost of the proposed procedure is dominated by the need to solve $N_{\mathbf{tr}} \times N_p$ nonlinear static problems, or $N_{\mathbf{tr}}$ as many static problems as would be required to create a single ICE ROM. However, this procedure is offline and each static load case could be computed in parallel. Note that once one has computed the set of static solutions $\mathbf{D}_{\text{tr}}$, it is relatively inexpensive to go through several iterations of the algorithm for computing and evaluating the GPR ROM.

It should be noted that it is critical that the training data samples capture the FEM parameter set adequately. The range for each FEM parameter should encompass the range of interest, as there is no reason to expect that the GP model will be able to extrapolate much beyond this range. Furthermore, the training data should contain sufficient samples in the range $[\mathbf{p}_{\min}, \mathbf{p}_{\max}]$ to capture variation in the FEM force displacement data $\mathbf{D}_{tr}$, and hence in the ROM coefficients $\boldsymbol{\Theta}_r$. The ROM interpolates between the training data using Eq. (14), and so any discontinuities or large variations that are not captured by the training data will lead to errors. In the examples shown in the following section, training data was sampled with a sufficient number to ensure that the mean predictions of the trained GPR ROM were continuous with respect to the varying FEM parameters. (i.e., see Figs. 4–7 and 11–13). While this does not prove that the training data is adequate, it provides some level of assurance. One must rely on engineering judgment for further verification or else augment the training data further until one is satisfied that the GPR ROM can interpolate between them accurately.

3. Numerical studies

The GPR ROM approach was numerically tested on a few thin structures that are well known to exhibit geometric nonlinearity. The GPR ROM was first applied to a flat beam to test how the data-driven ROM captures the underlying physics and the variability with respect to a single FEM parameter. A curved beam is then used to show how the method performs on a structure that exhibits more complicated nonlinear behaviors such as snap-through, and where it is much more difficult to fit an accurate ROM and to determine how many terms should be retained in the ROM.

The accuracy and efficacy of the GPR ROMs were evaluated using their nonlinear normal modes (NNMs). An NNM is a powerful metric for comparing models, as it captures the full range of near-resonant nonlinear responses that a structure can exhibit, from small to large amplitudes. They are also independent of the temporal or spatial pattern of the loading applied to the system [40]. In this work, the NNMs were computed by using the multi-harmonic balance (MHB) method introduced in [41]. All the FE modeling and the numerical methods for computing static/dynamics responses were implemented with a Matlab-based nonlinear FEA package, OSFern (https://bitbucket.org/cvandamme/osfern).

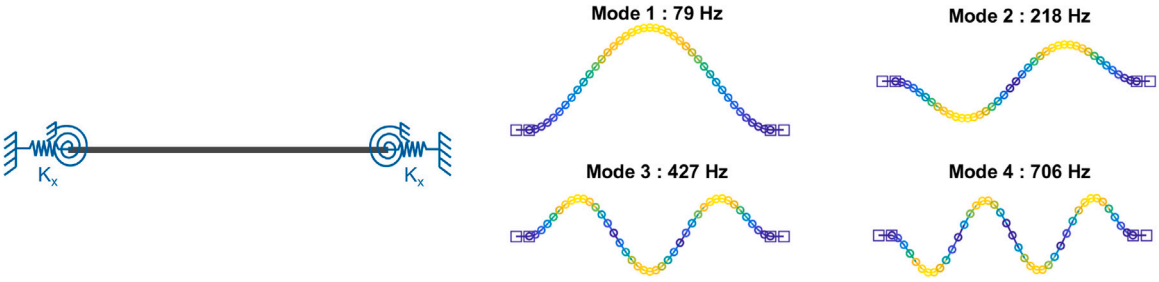

Fig. 2. The flat beam model and its dominant modes. The modes were computed with the nominal beam having the axial spring stiffness $K_x = 5.0 \times 10^5$ lbf in^{-1}.

Table 1
The GPR ROM framework parameters for the flat beam model.

Number of training sets (N_{tr})	20
Number of load cases per a training set (N_p)	7
Random force scaling range ($[f_{\min}, f_{\max}]$)	[0.25, 0.75] × beam thickness
Number of test sets (N_{te})	900
Maximum allowable predictive STD per mode ($\overline{\sigma}_{\max}$)	[0.07, 0.07]
Maximum allowable number of ROM coefficients ($N_{\text{nl, max}}$)	8

3.1. Flat beam

The flat, geometrically nonlinear beam used here has been studied in many prior works. The nonlinearity arises as a large transverse motion induces axial stretch in the beam, causing coupling between the bending and membrane modes and hardening the stiffness of the structure [18,42,43]. The flat beam model used here is identical to the beam model in [27], which has axial springs attached to approximate the stiffness of the boundaries. The nominal beam model was 228.6 mm in length, 12.7 mm in width, 0.787 mm in thickness, and was composed of 40 2-node beam elements. The Young's modulus was 204.8 GPa, Poisson's ratio was 0.29, and the mass density was 7870 kg m^{-3} to approximate steel. The flat beam model and the first four bending modes are illustrated in Fig. 2.

3.1.1. Training GPR ROM of flat beam

In this case study, a GPR ROM of the flat beam was designed to incorporate the variation of boundary stiffness, which is typically one of the most uncertain parameters when modeling structures such as this. A wide range of the boundary stiffness, from soft to nearly clamped, was considered in the GPR ROM, by choosing the lower and upper bounds of the axial spring stiffness $K_x \in [K_{x,\min}, K_{x,\max}] = [1.0 \times 10^4, 5.0 \times 10^5]$ lbf in^{-1}. Within the given range, the variation of the stiffness K_x significantly impacted the nonlinear coefficients of the ROM, while not changing the linear frequencies of any of the bending modes that made up the ROM. Note that the variation in the boundary stiffness in the given range did not severely change the mode shapes. The mode shapes varied slightly in the peaks and slopes, but consistently followed the mode shapes of the nominal beam model in Fig. 2. The training sets of varying K_x were uniformly sampled within the bounds and the number of samples was $N_{\text{tr}} = 20$. When generating the training sets, the signs of the mode shapes of each set were adjusted to assure that they were consistent with those of the nominal FEM to prevent the possible mismatching in the training sets. The reduced basis of the GPR ROM included Mode 1 and 3 (2-DOF ROM), and the correspondingly defined parameters for the GPR ROM framework are presented in Table 1.

Note that only $N_{tr} N_p = 140$ static load cases are needed to train the model, and the $N_{te} = 900$ test sets are computed by evaluating the GPR ROM for various FEM parameter vectors and so are inexpensive to compute. The trained GPR ROM was evaluated using 900 uniformly distributed test sets and the predicted mean and confidence interval of the GP model of each nonlinear ROM coefficient are shown in Figs. 3 and 4. It is worth noting that the confidence intervals shown are the 95% intervals (or the $\pm 2\sigma$ bounds) computed using the conditional covariance in Eq. (17); the actual errors in fitting a GPR ROM to the training data may not be Gaussian and could contain both epistemic and aleatory uncertainty so these should not be considered to be true statistical bounds. Fig. 3 illustrates that all the quadratic coefficients are very uncertain and have large variances centered around zero, which are mainly due to computational noise from the ICE ROM fitting process as well as the random force scaling. The predictive STDs of the first mode's nonlinear coefficients are presented in Table 2, which also support the significant uncertainty of the quadratic terms. Furthermore, any changes in these terms with respect to the axial spring stiffness are smaller than the uncertainty, and hence they can be removed from the ROM. This is as expected, as the geometric nonlinearity of a flat, symmetric beam is known to not contain any quadratic stiffness effects. On the contrary, the cubic coefficients captured the variation of the FEM parameters with small uncertainties, as can be found in Fig. 4 and Table 2. The coefficients were observed to transition smoothly from small to large values as the axial spring stiffness varied. Fig. 5 demonstrates the GPR ROM prediction for the cubic coefficients when applying a constant force scaling factor ($f_r = 0.5$) instead of a random force scaling factor for training the GPR ROM. As the sensitivity with respect to the force scaling was neglected in the training, the uncertainty was dramatically reduced (e.g., see $\beta_{1,113}$ and $\beta_{3,113}$). The

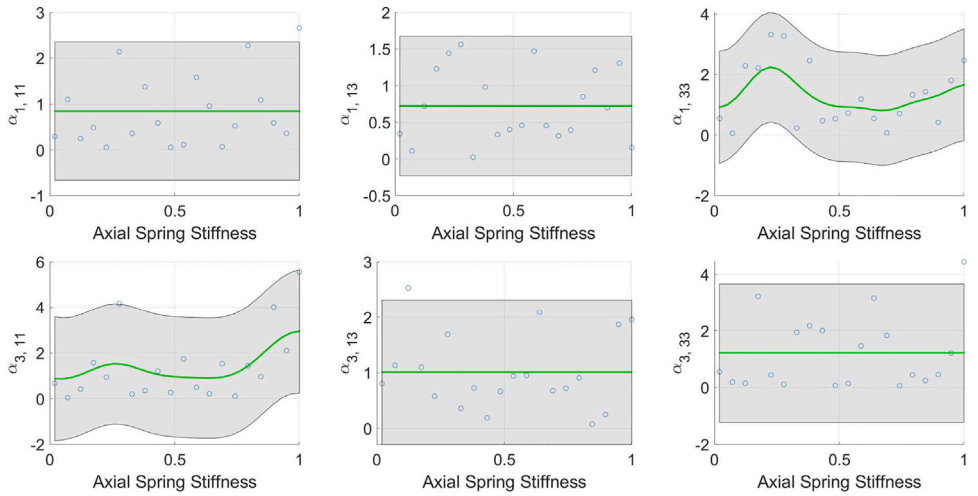

Fig. 3. The GPR ROM prediction for the quadratic coefficients at the first iteration ($N_{\mathrm{nl}} = 14$): trained observations (blue circles), mean prediction (green curve), and its 95% predictive confidence (gray surface). The nonlinear ROM coefficients and the axial spring stiffness are normalized by the nominal values.

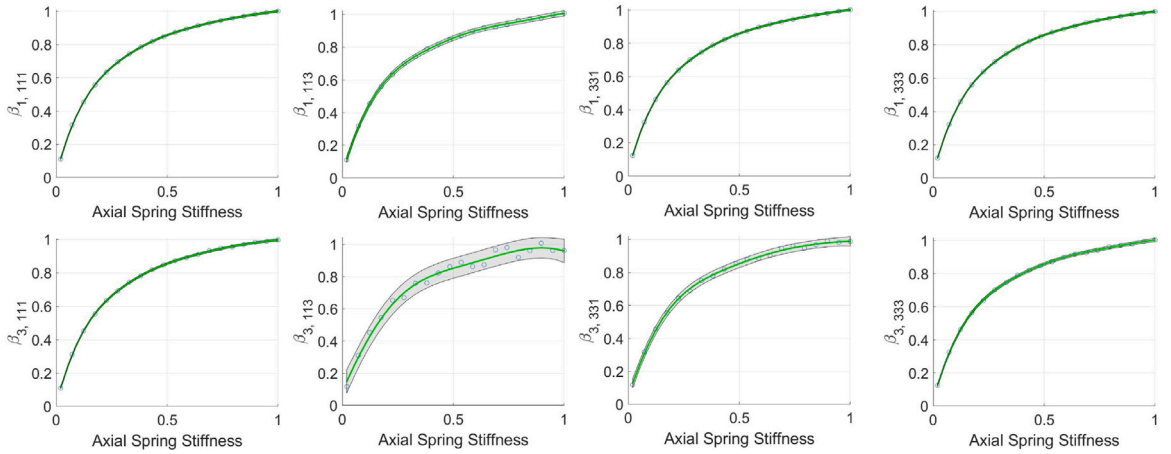

Fig. 4. The GPR ROM prediction for the cubic coefficients at the first iteration ($N_{\mathrm{nl}} = 14$): trained observations (blue circles), mean prediction (green curve), and its 95% predictive confidence (gray surface). Note that the results after the second iteration ($N_{\mathrm{nl}} = 8$) were visually indistinguishable from these.

results indicate that the uncertainty of the coefficients was mainly due to their sensitivity to the force scaling factor, while the FEM variation produced negligible uncertainty.

Based on the degree of uncertainty estimated for each nonlinear coefficient, the GPR ROM algorithm removed all the quadratic terms and kept the cubic terms in the filtering stage. The reduced GPR ROM ($N_{\mathrm{nl}} = 8$) functioned the same as the full GPR ROM ($N_{\mathrm{nl}} = 14$) as can be inferred from Table 2, and the mean predictive STD of the GPR ROM $\overline{\sigma}_{\mathrm{GPR}}$ significantly reduced from 0.393 to 0.009, indicating that the ROM became small but robust with respect to the force scaling factor. The GPR ROM could be further filtered to have $N_{\mathrm{nl}} = 6$, and the resulting GP models of the nonlinear ROM coefficients are shown in Fig. 6. A slight increase of uncertainty could be seen for the cubic terms, which was also found with increased predictive STDs ($\overline{\sigma}_{\mathrm{y}}$) in Table 2. This implied that the robustness of the GPR ROM with respect to the force scaling factor has started to decrease. If one were to seek to reduce the number of GPR ROM coefficients further, to $N_{\mathrm{nl}} = 4$ and 2, the uncertainty would increase even more, as indicated in Table 2. Fig. 7 illustrates the GPR ROM prediction when applying a constant force scaling factor ($f_r = 0.5$) for training the GPR ROM of $N_{\mathrm{nl}} = 6$. This again supports the fact that the uncertainty of the GPR ROM to the FEM variation was ignorable. It is important to note that while using a constant force scaling resulted in a GPR ROM with negligible uncertainty, the GPR ROM would not necessarily be accurate. As shown by Kuether et al. [15], if the value of the force scaling was not chosen optimally the NNMs computed with such a ROM could be significantly in error. Hence, the variances estimated in the GPR ROM fitting process are only meaningful if the load cases used to create the ROMs are sufficiently rich.

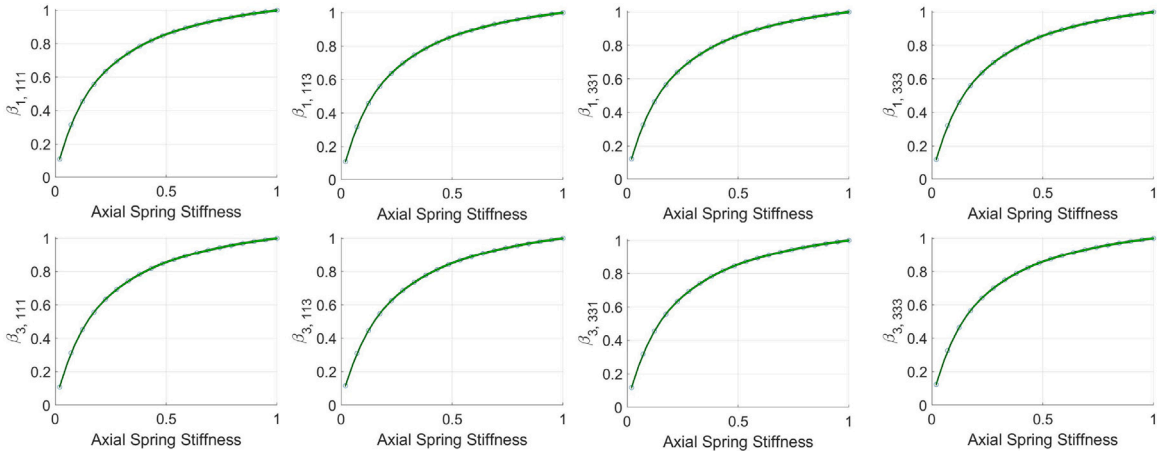

Fig. 5. The GPR ROM prediction for the cubic coefficients when the force scaling factor applied to all the training sets was constant ($f_r = 0.5$) for training the GPR ROM: trained observations (blue circles), mean prediction (green curve), and its 95% predictive confidence (gray surface). The results represent the prediction both at $N_{\text{nl}} = 14$ and $N_{\text{nl}} = 8$, which were visually indistinguishable.

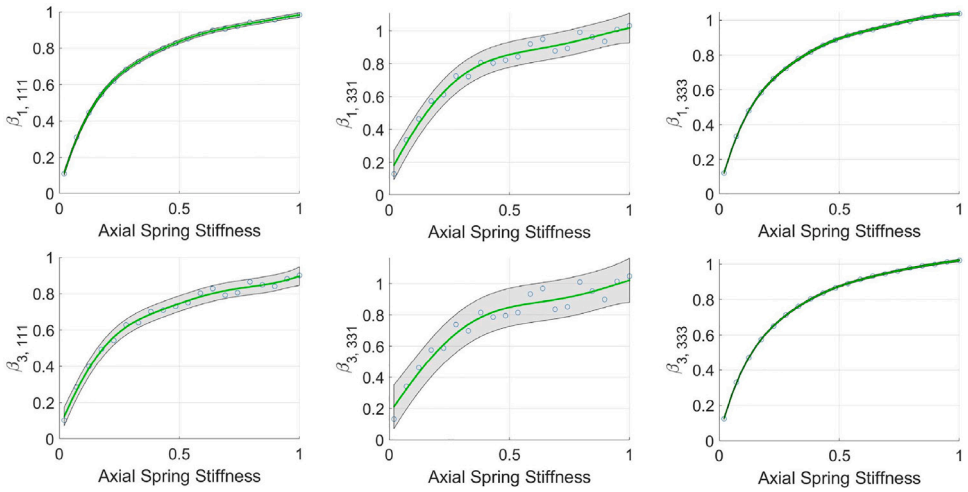

Fig. 6. The GPR ROM prediction for the cubic coefficients at the third iteration ($N_{\text{nl}} = 6$): trained observations (blue circles), mean prediction (green curve), and its 95% predictive confidence (gray surface).

Table 2
The predictive STDs of the nonlinear ROM coefficients ($\overline{\sigma}_{\text{y}}$) of Mode 1 and their mean ($\overline{\sigma}_{\text{GPR},1}$) of the GPR ROM. The STDs are estimated using the normalized values of the nonlinear ROM coefficients.

	$\alpha_{1,11}$	$\alpha_{1,13}$	$\alpha_{1,33}$	$\beta_{1,111}$	$\beta_{1,113}$	$\beta_{1,133}$	$\beta_{1,333}$	$\overline{\sigma}_{\text{GPR},1}$
Iteration 1 ($N_{\text{nl}} = 14$)	0.770	0.485	0.924	0.003	0.008	0.003	0.003	0.314
Iteration 2 ($N_{\text{nl}} = 8$)	–	–	–	0.003	0.008	0.003	0.003	0.004
Iteration 3 ($N_{\text{nl}} = 6$)	–	–	–	0.006	–	0.040	0.004	0.016
Iteration 4 ($N_{\text{nl}} = 4$)	–	–	–	0.034	–	–	0.091	0.063
Iteration 5 ($N_{\text{nl}} = 2$)	–	–	–	0.092	–	–	–	0.092

3.1.2. Evaluation of GPR ROM of flat beam using NNMs

The accuracy and robustness of the GPR ROMs were evaluated using their NNMs. The NNM backbone curves were computed by applying the MHB method using five harmonics. In this work, NNMs are represented on the frequency–energy plane, in which any point on the curves represents a frequency that corresponds to the minimal period of periodic response at a given energy (i.e., a sum of kinetic and potential energy of the nonlinear system). The NNM curves captured by the GPR ROMs are illustrated in Fig. 8. The NNMs were computed from the mean prediction of the GPR ROMs at each given boundary stiffness, using the conditional mean in Eq. (17). The GPR ROM could estimate the variability of nonlinear responses for a wide range of boundary stiffness. For example, when the beam was at total conserved energy of 0.001 J, the GPR ROM was able to capture about 15 Hz frequency shift of the first

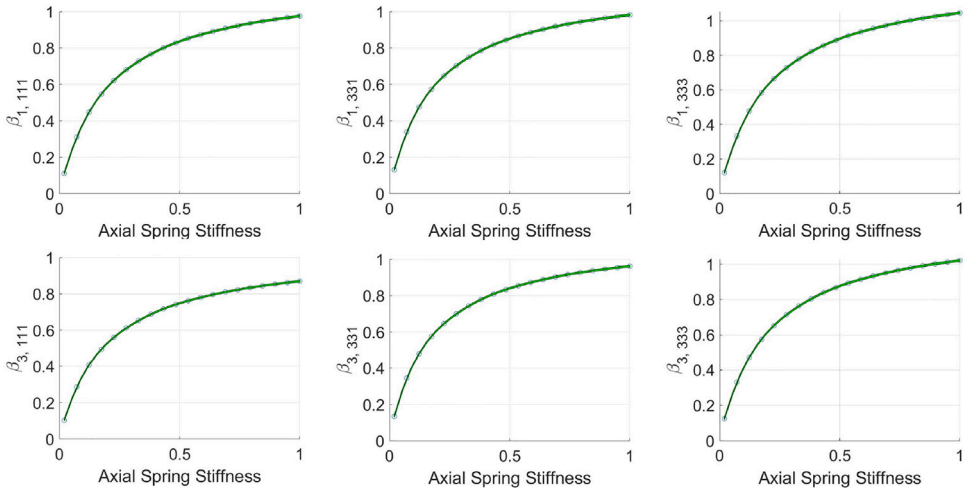

Fig. 7. The GPR ROM prediction for the cubic coefficients when the force scaling factor applied to all the training sets was constant ($f_r = 0.5$) for training the GPR ROM of $N_{\mathrm{nl}} = 6$: trained observations (blue circles), mean prediction (green curve), and its 95% predictive confidence (gray surface).

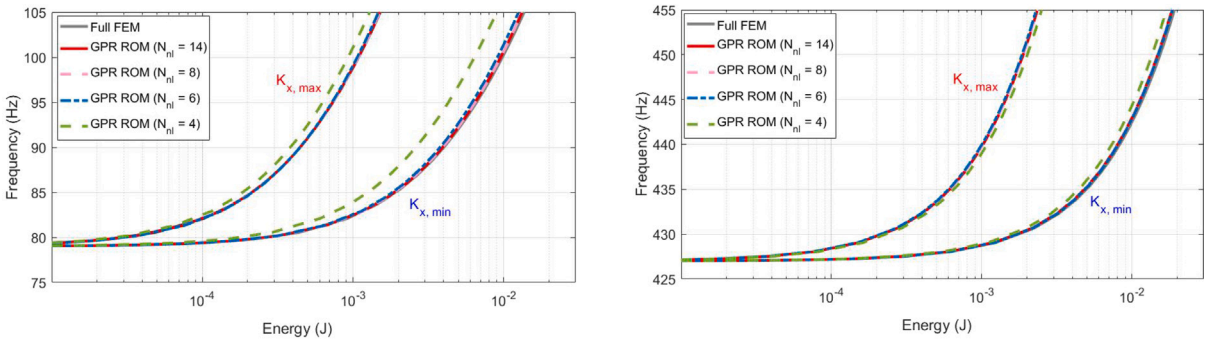

Fig. 8. The 1st and 3rd NNM curves of the flat beam computed from the mean prediction of the GPR ROMs of various orders. For each order N_{nl}, two NNMs were computed, one for $K_{x,\mathrm{min}}$ and one for $K_{x,\mathrm{max}}$. This illustrates how a single ROM captures wide variation in this parameter of the FEM.

NNM that is due to the change of the boundary stiffness. Also, it is important to note that any NNM curve within the range could be estimated by using a ROM from the regression model; it is not necessary to solve additional static load cases to train a new ROM.

The accuracy of the GPR ROM was evaluated at two extreme boundary conditions. The NNM curves closely matched the reference NNM of the full FEM when $N_{\mathrm{nl}} \geq 6$, and started to break down from $N_{\mathrm{nl}} = 4$. This agrees well with the observation that the predictive variance of the $N_{\mathrm{nl}} = 8$ or $N_{\mathrm{nl}} = 6$ ROM coefficients was very low. The fact that the NNMs match so closely implies that there would also be an excellent agreement between a wide range of forced or free dynamic responses in which this mode is dominant. Note that the error from the reference curves was relatively small for the 3rd NNM, regardless of having large uncertainty in the GPR ROMs (e.g., $N_{\mathrm{nl}} = 4$). This was because the flat beam entails relatively weak modal coupling, as illustrated in our recent study [43], so a small number of coefficients could be enough to capture some of the nonlinear dynamic responses.

The predictive confidence for estimating the NNMs when using the GPR ROMs is also shown in Fig. 9. The confidence bounds of the NNMs were computed from the Gaussian sample sets generated at the upper and lower bounds of the 95% confidence interval of the GPR ROM prediction, using the conditional covariance in Eq. (17). The uncertainty of GPR ROM was commensurably translated to the uncertainty of the nonlinear response, and the confidence intervals dramatically increased from $N_{\mathrm{nl}} \leq 4$. As expected, there is a trade-off between having highly certain prediction and reducing the size of the ROM. It can thus serve as a powerful indicator for defining the optimal ROM coefficient set, depending on whether one is more interested in robustness or computational efficiency in the application in question. This highlights one very appealing feature of the GPR ROM, as it allows one to not only predict the ROM but the uncertainty in the ROM due to the training data.

3.2. Curved beam

Curved beam structures exhibit complex nonlinear behaviors such as snap-through instability, and also entail relatively stronger modal coupling between low and high frequency modes compared to flat beam structures [43,44]. In this study, the GPR ROM

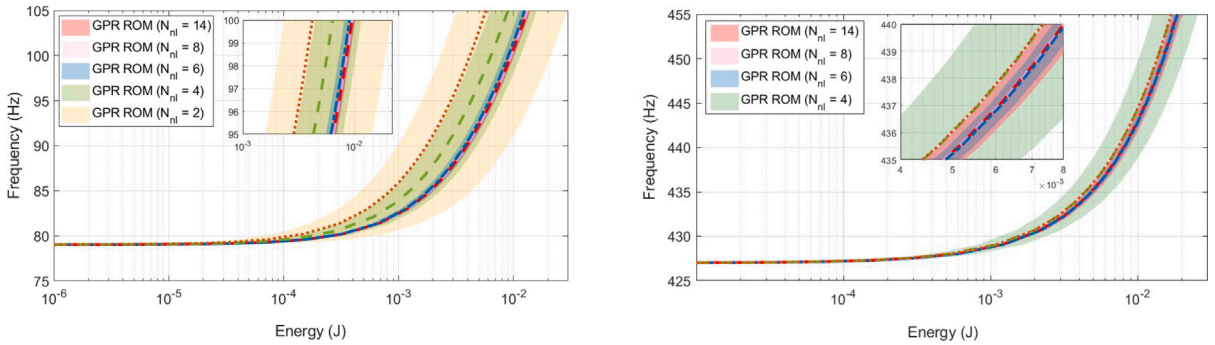

Fig. 9. The predictive confidence interval (95%) of the 1st and 3rd NNM curves estimated from the GPR ROMs at $K_{x,\min}$.

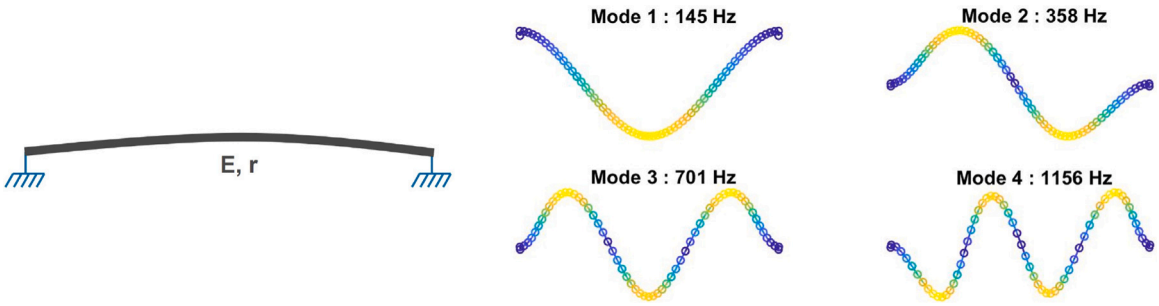

Fig. 10. The nominal curved beam model and its dominant modes.

was applied and tested on a curved beam model, which approximates the 3D printed structure tested in [27]. The beam model was composed of 62 beam elements (183 free DOF), and the dimensions were 180 mm in length, 3175 mm in radius of curvature, 8.32 mm in width, and 2.60 mm in thickness. The material properties of the model followed the nominal values of polylactic acid (PLA), such that the Young's modulus was 3.10 GPa, the Poisson's ratio was 0.33, and the density was 1248 kg m^{-3}. The two ends of the beam were assumed to be stiff but not fixed, so were approximated with vertical beams that had the same material property (PLA) and length of 10 mm, width of 30 mm, and thickness of 10 mm. Fig. 10 illustrates the nominal curved beam model and its first four bending modes.

3.2.1. Training GPR ROM of curved beam

The design parameters for the curved beam GPR ROM were the Young's modulus (E) and the radius of curvature (r) of the main beam. These were treated as parameters because they entail significant uncertainties due to the manufacturing variability, and they also have a significant effect on the dynamic response. The upper and lower bound of both of these parameters were taken to be 150% and 50% of their nominal values, so that the GPR ROM would capture the system for this range of values. From the given range of the two uncertain FEM parameters, 10 uniformly distributed samples were selected from each FEM parameter and combined to construct one hundred training sets ($N_{\text{tr}} = 100$). Similar to the flat beam case, the mode shapes of all the training sets matched well with those of the nominal model, with minor variations in the peaks and slopes. When generating the training sets, the signs of the mode shapes were forced to be the same as those of the nominal curved beam model, so the modal information was consistent in the training sets. It is worthwhile to note that the mode shapes in our cases did not reorder nor were there large changes in the mode shapes, but this would certainly be an issue for more complicated structures and should be addressed in future works. In such cases, the GPR ROM framework may need an additional pre-processing, (e.g., subgrouping the training sets based on the mode shapes and then applying GPR fitting to each subgroup), which is left to be explored in a future work.

The training sets were used to train a 3-DOF GPR ROM consisting of Modes 1, 2, and 3. The corresponding GPR ROM framework parameters are presented in Table 3. Compared to the previous flat beam example, the complexity of the GPR ROM model was exponentially increased by incorporating two-dimensional design variation in the FEM, and having a three mode basis in the ROM. This resulted in a significant increase in the total number of static load cases, as can be found in Table 3. The random force scaling range ($[f_{\min}, f_{\max}]$) was chosen wide enough to sufficiently capture the nonlinear dynamic behavior of the curved beam at large deformations, which will be further discussed in the following sections.

Fig. 11 illustrates the predicted means and confidence intervals of the linear frequencies estimated by the uniformly sampled test set $\mathbf{P}_{\text{te}}$. The GP models capture smooth variation in the linear frequencies due to changes in the FEM parameters with almost no uncertainty, indicating that they were not corrupted by any noise and accurately modeled using sparse training data. The results

Table 3
The GPR ROM framework parameters for the curved beam model.

Number of training sets (N_{tr})	100
Number of load cases per a training set (N_p)	16
Random force scaling range ($[f_{\min}, f_{\max}]$)	$[0.25, 3.00]\times$ beam thickness
Number of test sets (N_{te})	900
Maximum allowable predictive STD per mode ($\overline{\sigma}_{\max}$)	[0.10, 0.10, 0.30]
Maximum allowable number of ROM coefficients ($N_{\text{nl, max}}$)	24

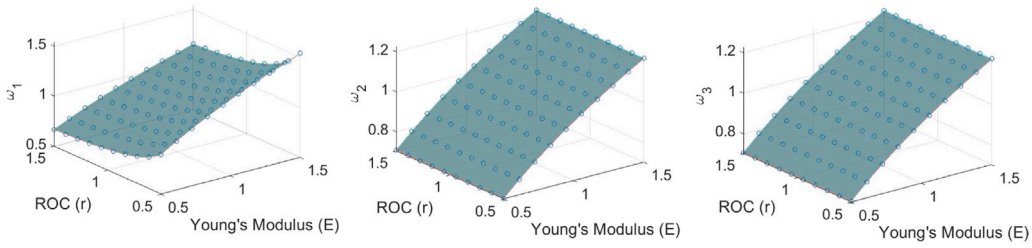

Fig. 11. The GPR ROM prediction for the linear frequencies: trained observations (blue circles), mean prediction (gray surface), and its upper bound (cyan surface) and lower bound (red surface) of 95% predictive confidence. The linear frequencies and the FEM parameters are normalized by the nominal values.

showed that the radius of curvature has a relatively small impact especially on the second and third linear frequencies, while the variation of Young's modulus significantly changes the linear frequencies.

Some GP models of resonant and non-resonant nonlinear coefficients were also evaluated and are depicted in Fig. 12. The resonant terms were discussed in [24], in which the cubic resonant terms are typically defined as $q_r q_i{}^2$ in the rth modal equation, where q_i can be any modal coordinate. The results in Fig. 12 revealed that the resonant coefficients were relatively certain and accounted for the variation of the design parameters well. For example, $\alpha_{1,11}$ increased quadratically or at most cubically to the increase of the radius of curvature while the coefficient was linearly proportional to the Young's modulus. The variation of Young's modulus also linearly propagated to the variation of $\beta_{1,111}$, but the variation of radius of curvature had no impact on this cubic term. On the other hand, the non-resonant terms had large prediction variances, revealing that they were very sensitive to the random force level used when estimating them, and thus were subjected to filtering by the GPR ROM algorithm. This corresponded well with the recent observation of Shen et al. [24], where they found the non-resonant terms to contribute less to capturing the system's nonlinearity.

The curved beam GPR ROM was trained through the proposed framework, and after 7 iterations, the number of nonlinear coefficients N_{nl} reduced from 48 to 21. The mean predictive STD of GPR ROM $\overline{\sigma}_{\text{GPR}}$ also substantially reduced from 0.232 to 0.060, indicating that the GPR ROM became much more robust as the size was reduced by more than 50%. The predictive STD of the resulting optimal GPR ROM can be also found in Table 4.

3.2.2. Effect of force scaling bounds on GPR ROM

The random force scaling contributes to the independent noise term ϵ_n in Eq. (15) for the GPR ROM, and the noise becomes significant for the load-sensitive nonlinear ROM coefficients. The case study investigated the effect of force scaling on the GPR ROM by testing multiple sets of different force scaling bounds for training a GPR ROM. Fig. 13 demonstrates some nonlinear GPR ROM coefficients trained using the reduced random force scaling bounds $[f_{\min}, f_{\max}] = [0.25, 0.75] \times$ beam thickness. Compared to the GP models applied by $[f_{\min}, f_{\max}] = [0.25, 3.00] \times$ beam thickness shown in Fig. 12, the predictive confidence interval has significantly decreased, particularly for the non-resonant coefficients. It can be inferred that as the range of applied loads increases, the static solution sets $\mathbf{D}_{\text{tr}}$ include larger deformations. This potentially increases the load-sensitive noise, consequently increasing the predictive variance of GPR ROM.

The case study applied five different force scaling bounds to train the GPR ROMs, and the predictive STDs of the nonlinear coefficients of the resulting optimal GPR ROMs are presented in Table 4. Note that the nonlinear coefficients kept in the GPR ROM were mostly the same between the cases with different force scaling bounds. The GPR ROM was robust enough, so even when the GPR ROM was computed using a smaller force scaling, it was able to evaluate and distinguish relatively uncertain coefficients from the certain ones in that ROM. The results again show that the uncertainty of the GPR ROM tends to increase as the force scaling range increases. When the force scaling range was larger, the nonlinear terms that are less impactful (e.g., most of the non-resonant terms) were more uncertain relative to the dominant terms (e.g., mostly the resonant terms), as can be observed by comparing Figs. 12 and 13. Hence, it appears to be advisable to use a larger force range so that it becomes easier to filter out these redundant coefficients.

All the resonant terms, except $\beta_{3,113}$ in Mode 3, showed low predictive uncertainty and were retained in the optimal GPR ROM. This supports the fact that they significantly contribute to forming a ROM to capture the system's nonlinearity. It is also important to note that a few non-resonant terms were still kept in the optimal ROM. It can be inferred that they are less significant but still have a small contribution to the ROM in terms of accuracy and reducing uncertainty.

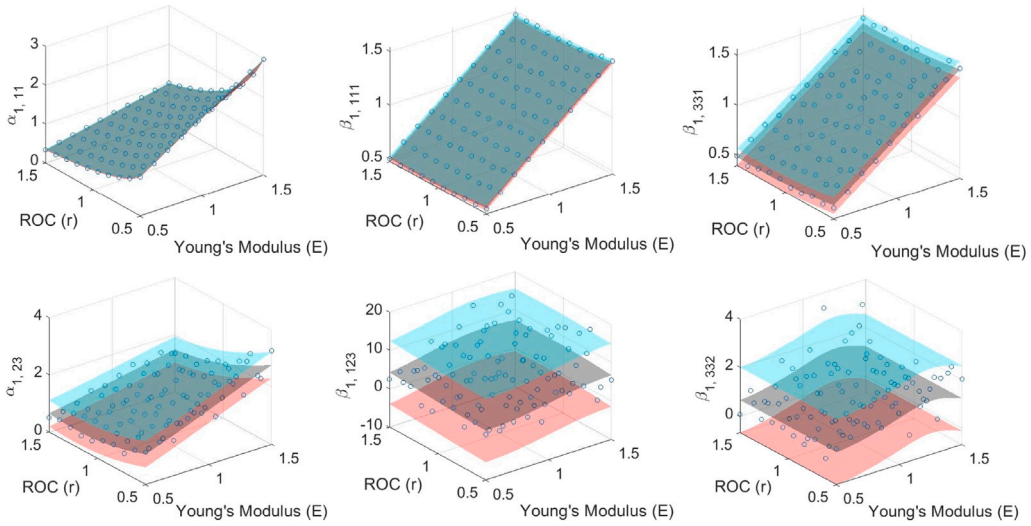

Fig. 12. The GPR ROM prediction for some resonant (top) and non-resonant (bottom) nonlinear terms when subjected to random force scaling bounds $f_r \in [0.25, 3.00] \times$ beam thickness: trained observations (blue circles), mean prediction (gray surface), and its upper bound (cyan surface) and lower bound (red surface) of 95% predictive confidence. The nonlinear ROM coefficients and the FEM parameters are normalized by the nominal values.

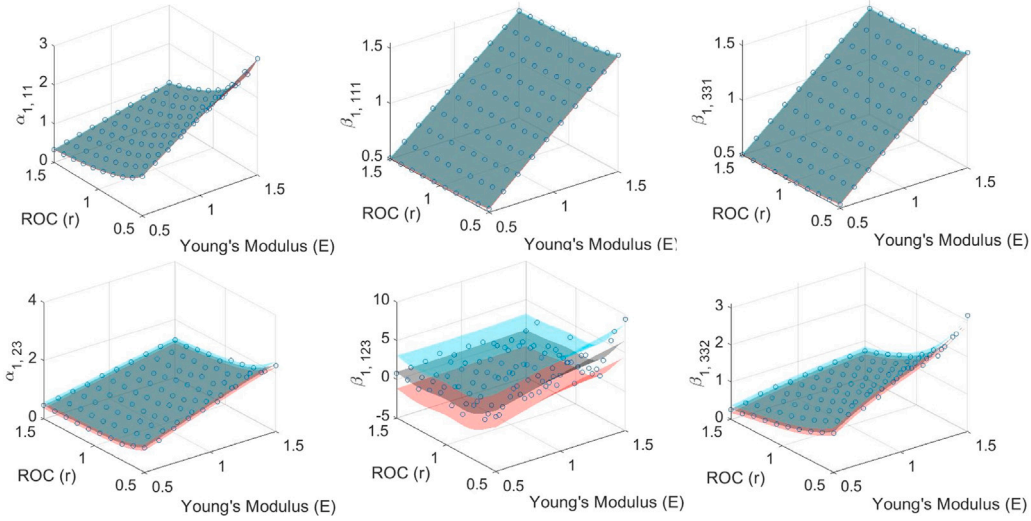

Fig. 13. The GPR ROM prediction for some resonant (top) and non-resonant (bottom) nonlinear terms when subjected to random force scaling bounds $f_r \in [0.25, 0.75] \times$ beam thickness: trained observations (blue circles), mean prediction (gray surface), and its upper bound (cyan surface) and lower bound (red surface) of 95% predictive confidence. The nonlinear ROM coefficients and the FEM parameters are normalized by the nominal values.

3.2.3. Evaluation of GPR ROM of curved beam using NNMs

The NNMs of the curved beam GPR ROMs were computed using the MHB method with five harmonics. The reference NNM backbone curves were computed using an ICE ROM with 10 modes, which was thought to have a large enough modal basis to accurately capture the NNMs. Fig. 14 shows the resulting NNMs from the GPR ROMs of various sizes when subjected to the force scaling $f_r \in [0.25, 3.00] \times$ beam thickness. The GPR ROMs accurately captured the nonlinear responses propagated from the design variation ranging from $(\mathrm{E}, \mathrm{r})_{\min}$ to $(\mathrm{E}, \mathrm{r})_{\max}$. Interestingly, the softening–hardening behavior at $(\mathrm{E}, \mathrm{r})_{\min}$ turns to pure hardening at $(\mathrm{E}, \mathrm{r})_{\max}$, a feature that is captured by the GPR ROM. The GPR ROM could also accurately describe the variation of hardening NNMs at higher frequencies in Mode 3, which covers nearly 300 to 400 Hz frequency shift as the FEM parameters vary.

The accuracy of GPR ROMs was preserved even when reducing the number of nonlinear coefficients by more than 50%, revealing that the 3-mode ROM contains a significant number of redundant coefficients that can be neglected while still accurately capturing the nonlinear responses. Note that the accuracy aligned well with the predictive variance estimated in the GPR ROM framework, as was also the case in the flat beam case study. While the optimal GPR ROM ($N_{\mathrm{nl}} = 21$) maintained a satisfactory accuracy, further reduction of nonlinear coefficients induced larger GPR ROM predictive variance and started to increase error for capturing the

Table 4
The predictive STDs of the nonlinear coefficients ($\bar{\sigma}_y$) of the GPR ROM trained with various force scaling bounds. The STDs are estimated using the normalized values of the nonlinear ROM coefficients.

(a) Mode 1

$[f_{min}, f_{max}]$	$\alpha_{1,11}$	$\alpha_{1,22}$	$\alpha_{1,33}$	$\alpha_{1,12}$	$\alpha_{1,13}$	$\alpha_{1,23}$	$\beta_{1,111}$	$\beta_{1,112}$	$\beta_{1,113}$	$\beta_{1,221}$	$\beta_{1,222}$	$\beta_{1,223}$	$\beta_{1,331}$	$\beta_{1,332}$	$\beta_{1,333}$	$\beta_{1,123}$	$N_{nl,1}$
[0.25, 0.75]	0.016	0.009	0.008				0.017			0.013			0.018		0.053		7
[0.25, 1.50]	0.017	0.006	0.039				0.015			0.006		0.056	0.060		0.040		8
[0.25, 2.00]	0.019	0.006	0.045				0.020			0.007		0.063	0.066		0.048		8
[0.25, 3.00]	0.027	0.019	0.083				0.027			0.021			0.088		0.060		7
[0.10, 3.00]	0.017	0.018	0.074				0.018			0.021			0.075		0.046		7

(b) Mode 2

$[f_{min}, f_{max}]$	$\alpha_{2,11}$	$\alpha_{2,22}$	$\alpha_{2,33}$	$\alpha_{2,12}$	$\alpha_{2,13}$	$\alpha_{2,23}$	$\beta_{2,111}$	$\beta_{2,112}$	$\beta_{2,113}$	$\beta_{2,221}$	$\beta_{2,222}$	$\beta_{2,223}$	$\beta_{2,331}$	$\beta_{2,332}$	$\beta_{2,333}$	$\beta_{2,123}$	$N_{nl,2}$
[0.25, 0.75]		0.015	0.013	0.006		0.010		0.007			0.004			0.003		0.006	8
[0.25, 1.50]		0.016	0.020	0.009		0.031		0.014			0.009			0.005		0.016	8
[0.25, 2.00]		0.020	0.024	0.013		0.033		0.018			0.010			0.006		0.021	8
[0.25, 3.00]		0.032		0.022		0.036		0.026			0.015			0.021		0.050	7
[0.10, 3.00]		0.022		0.019		0.032		0.024			0.013			0.020		0.087	7

(c) Mode 3

$[f_{min}, f_{max}]$	$\alpha_{3,11}$	$\alpha_{3,22}$	$\alpha_{3,33}$	$\alpha_{3,12}$	$\alpha_{3,13}$	$\alpha_{3,23}$	$\beta_{3,111}$	$\beta_{3,112}$	$\beta_{3,113}$	$\beta_{3,221}$	$\beta_{3,222}$	$\beta_{3,223}$	$\beta_{3,331}$	$\beta_{3,332}$	$\beta_{3,333}$	$\beta_{3,123}$	$N_{nl,3}$
[0.25, 0.75]		0.011	0.045							0.051		0.009	0.041		0.024		6
[0.25, 1.50]		0.067	0.108							0.098		0.032	0.051		0.022		6
[0.25, 2.00]		0.071	0.130			0.117				0.102		0.055	0.062		0.026		7
[0.25, 3.00]		0.111	0.178			0.130				0.127		0.077	0.082		0.032		7
[0.10, 3.00]		0.104	0.164			0.106				0.106		0.068	0.083		0.024		7

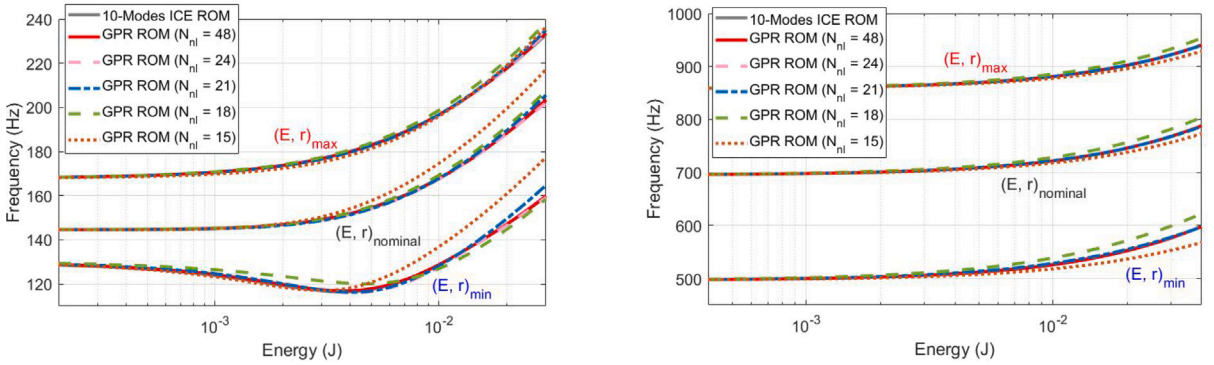

Fig. 14. The 1st and 3rd NNM curves of the curved beam computed from the mean prediction of the GPR ROMs using random force scaling bounds $f_r \in [0.25, 3.00] \times$ beam thickness.

NNMs. The predictive confidence for estimating the 1st NNMs when using the GPR ROMs is shown in Fig. 15, which also suggests that reducing the order of the GPR-ROM to fewer than 21 terms begins to significantly increase the uncertainty in the nonlinear response.

The effect of force scaling range on the predictive performance of the GPR ROM was estimated using NNM curves, as shown in Fig. 16. The GPR ROM created by applying random force scaling factors $f_r \in [0.25, 0.75] \times$ beam thickness was compared to the GPR ROM with $f_r \in [0.25, 3.00]$, in terms of accuracy for estimating the 1st NNMs. The differences between the predicted NNMs were quite small for all cases except for that with $N_{nl} = 18$, where the GPR ROM with $f_r \in [0.25, 3.00]$ seems to have a significant error in the snap through region. In the end it seems that the GPR ROM is not as sensitive to the range of force scaling as it is to the number of coefficients retained, and so one can use scaling ranges between $f_r \in [0.25, 0.75]$ and $f_r \in [0.25, 3.00]$ and focus attention on making sure that enough coefficients are retained in the ROM; the best practice is probably to choose $f_r = 0.25$ as the lower bound and to choose the upper bound to be approximately equal to the largest displacements that are expected.

The predictive confidence for estimating the 1st NNMs when using the GPR ROM of $f_r \in [0.25, 0.75] \times$ beam thickness is illustrated in Fig. 17. In the previous section, it was found that the predictive uncertainty of the GPR ROM was greater when the force scaling range was larger. However, the confidence intervals of some GPR ROMs applied by the larger force scaling range in Fig. 15 are even narrower than those of the GPR ROMs applied by the smaller force scaling range in Fig. 17, particularly at large deformations. Once again it appears that the method is insensitive to the range of force scaling as long as the nonlinearity is exercised to a sufficient extent. This also highlights the utility of using the GPR ROM to predict confidence intervals on the nonlinear responses such as these NNMs.

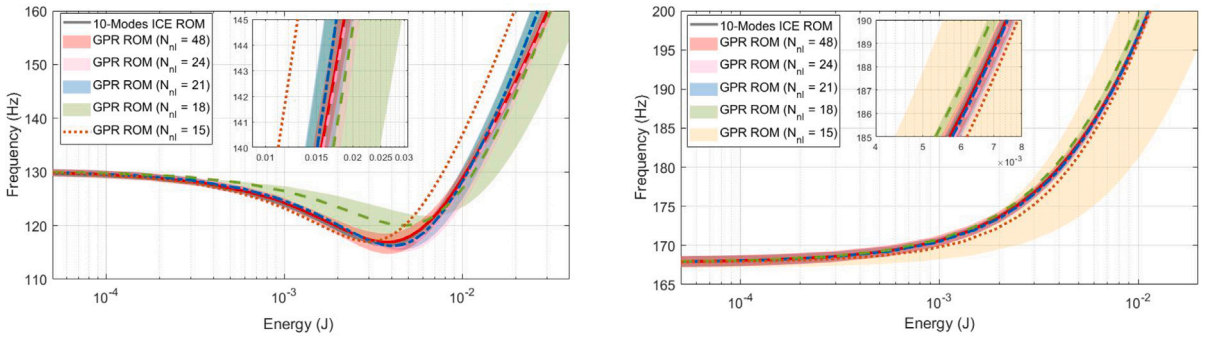

Fig. 15. The predictive confidence interval (95%) of the 1st NNM curves estimated from the GPR ROMs using random force scaling bounds $f_r \in [0.25, 3.00] \times$ beam thickness. The 1st NNM curves at (E, r) $_{\text{min}}$ (left) and (E, r)$_{\text{max}}$ (right).

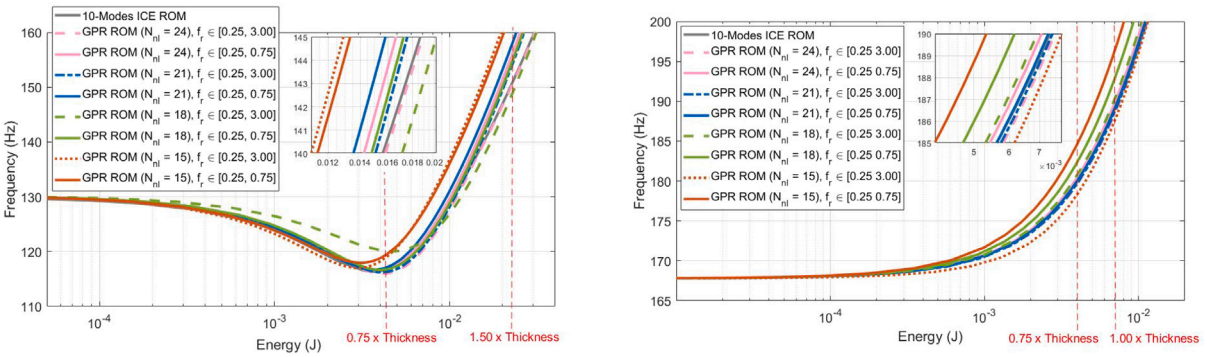

Fig. 16. The 1st NNM curves of the curved beam computed from the mean prediction of the GPR ROMs using random force scaling bounds $f_r \in [0.25, 0.75] \times$ beam thickness. The 1st NNM curves at (E, r)$_{\text{min}}$ (left) and (E, r)$_{\text{max}}$ (right). (The 10-mode ROM NNM curve at (E, r)$_{\text{max}}$ is completely overlapped by the curve of the GPR ROM of $N_{\text{nl}} = 21$, $f_r \in [0.25, 0.75] \times$ beam thickness.)

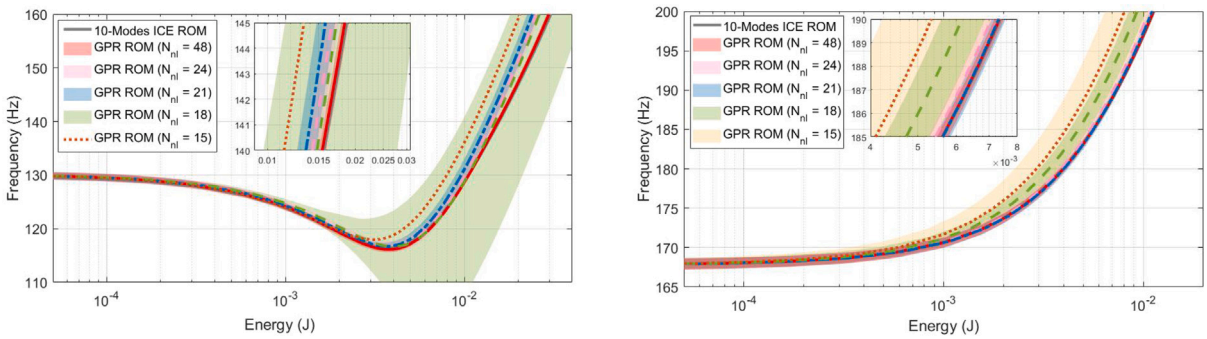

Fig. 17. The predictive confidence interval (95%) of the 1st NNM curves estimated from the GPR ROMs using random force scaling bounds $f_r \in [0.25, 0.75] \times$ beam thickness. The 1st NNM curves at (E, r)$_{\text{min}}$ (left) and (E, r)$_{\text{max}}$ (right).

3.2.4. Discussion on computational efficiency of GPR ROM

The case study was used to evaluate the computational efficiency of the GPR ROM and to compare it with that of a full FEM and a typical ROM (i.e., 3-DOF ICE ROM). The computations were performed on an Intel Core i7-7700 K 4.2 GHz quad-core computer with 64 GB of RAM. The comparison of computational time between different approaches is presented in Table 5. The offline stage for training GPR ROM required a relatively high computational cost, and this was due to computing a large number of static solutions $\mathbf{D}_{\text{tr}}$. That is, this case study computed 100 times as many load cases as would be minimally necessary to compute a typical ICE ROM. However, the cost was still small relative to that required to integrate the full-order dynamic equations. Also, note that this stage is entirely offline, and, if resources are available, it can be parallelized with perfect efficiency because each static load case is independent.

Table 5
The comparison of computational time (s) for training the curved beam models and integrating 10 s simulation under random loading. The sampling rate was 10,000 Hz.

	Full FEM	ICE ROM	GPR ROM
Offline ROM training	–	–	501.60
Online ROM computation	–	4.93	0.01
Time integration for 10 s	5652.84	8.87	8.86

In the online stage (in which the user might typically want a fast or even a real-time ROM), the GPR ROM could quickly generate an ICE ROM in less than a second for any given set of FEM parameters, whereas the ICE ROM approach needed to newly compute the static data to create a corresponding ROM. The GPR ROM was also tested to integrate the random responses of the curved beam, and it was revealed that the computational efficiency was the same as that of an ICE ROM, in that they are orders of magnitude faster than integrating the full FEM.

It should be noted that the computational efficiency of the GPR ROM will be amplified further when the parent FE model is composed of a large number of elements, and a ROM also requires a large number of modes to capture the nonlinear responses of that system. In such case, the trade-off between offline training and online prediction will become much more substantial.

4. Conclusion

This study proposed a new data-driven model reduction approach for geometrically nonlinear structures based on the Gaussian process regression method. To the best of the authors' knowledge, this is the first study to incorporate design variation in a geometrically nonlinear structure into a machine learning based reduced order model. By combining GPR with the well established ICR ROM, the governing physics of the problem are preserved in the form of polynomials in the modal coordinates and parameter variation in the FEM is efficiently captured by the mean and covariance terms in the GPR model. Thus, with a single GPR ROM one could compute the response of the FE model for any set of values of the parameters in the range of the training data. Similarly, if those parameters are known to be uncertain and not defined by a single value, then one could use the GPR ROM to efficiently compute the variability in the response due to the known distribution of those FEM parameters. The GPR ROM also provides a means to evaluate the sensitivity of nonlinear ROM coefficients with respect to the force scaling, and in the case studies presented here was able to reduce the set of nonlinear coefficients by filtering out any nonlinear coefficients that changed significantly as the force scaling changed. Hence, the proposed GPR ROM strategy has a built-in means for creating a small and robust ROM, which resolves a major limitation of the implicit condensation and expansion (ICE) method [15]. The proposed GPR ROM approach will be further tested as a short term future work on more realistic structures, e.g., exhaust cover plates and instrumental gongs, to evaluate its computational efficiency and robustness to represent the geometric nonlinearity of more complicated structures.

From a data-driven perspective, the GPR ROM could be efficiently pre-computed offline with a sparse set of training data, and at the online stage a ROM could be directly predicted for any new input FEM parameter set without any additional static analysis typically required for computing a ROM. In this respect, the GPR ROM can be a very powerful tool to be incorporated into nonlinear FEM updating (FEMU) tasks [9–11]. Using this approach, there would be no need to iterate on the Galerkin projection to correlate FEM to ROM, and the variation of the FEM is directly linked to the GPR ROM in the form of analytical sensitivity. This is expected to greatly accelerate nonlinear FEMU, and overcome a critical issue of recently developed ROM based model updating methods that do not bridge between the updated ROM and the actual design parameterized in the FEM [26–28]. The GPR ROM based FEMU will be further explored as a future work.

Declaration of competing interest

The authors declare that they have no known competing financial interests or personal relationships that could have appeared to influence the work reported in this paper.

Data availability

Data will be made available on request.

References

[1] P.F. Pai, A.H. Nayfeh, A fully nonlinear theory of curved and twisted composite rotor blades accounting for warpings and three-dimensional stress effects, Int. J. Solids Struct. 31 (9) (1994) 1309–1340.
[2] R. De Borst, M.A. Crisfield, J.J. Remmers, C.V. Verhoosel, Nonlinear Finite Element Analysis of Solids and Structures, John Wiley & Sons, 2012.
[3] E. Dowell, Nonlinear flutter of curved plates, AIAA J. 7 (3) (1969) 424–431.
[4] C. Mei, K. Abdel-Motagaly, R. Chen, Review of nonlinear panel flutter at supersonic and hypersonic speeds, Appl. Mech. Rev. 52 (10) (1999) 321–332, http://dx.doi.org/10.1115/1.3098919.
[5] M. Blair, R.A. Canfield, R.W. Roberts Jr., Joined-wing aeroelastic design with geometric nonlinearity, J. Aircr. 42 (4) (2005) 832–848.
[6] K.D. Murphy, D. Ferreira, Thermal buckling of rectangular plates, Int. J. Solids Struct. 38 (22–23) (2001) 3979–3994.

[7] M. Dokainish, K. Subbaraj, A survey of direct time-integration methods in computational structural dynamics—I. Explicit methods, Comput. Struct. 32 (6) (1989) 1371–1386.
[8] K. Subbaraj, M. Dokainish, A survey of direct time-integration methods in computational structural dynamics—II. Implicit methods, Comput. Struct. 32 (6) (1989) 1387–1401.
[9] S. Peter, A. Grundler, P. Reuss, L. Gaul, R.I. Leine, Towards finite element model updating based on nonlinear normal modes, in: Nonlinear Dynamics, Vol. 1, Springer, 2016, pp. 209–217.
[10] T. Hill, P. Green, A. Cammarano, S. Neild, Fast Bayesian identification of a class of elastic weakly nonlinear systems using backbone curves, J. Sound Vib. 360 (2016) 156–170.
[11] M. Song, L. Renson, J.-P. Noël, B. Moaveni, G. Kerschen, Bayesian model updating of nonlinear systems using nonlinear normal modes, Struct. Control Health Monit. 25 (12) (2018) e2258.
[12] M.P. Mignolet, A. Przekop, S.A. Rizzi, S.M. Spottswood, A review of indirect/non-intrusive reduced order modeling of nonlinear geometric structures, J. Sound Vib. 332 (10) (2013) 2437–2460.
[13] P. Tiso, E. Jansen, M. Abdalla, Reduction method for finite element nonlinear dynamic analysis of shells, AIAA J. 49 (10) (2011) 2295–2304.
[14] A.A. Muravyov, S.A. Rizzi, Determination of nonlinear stiffness with application to random vibration of geometrically nonlinear structures, Comput. Struct. 81 (15) (2003) 1513–1523.
[15] R.J. Kuether, B.J. Deaner, J.J. Hollkamp, M.S. Allen, Evaluation of geometrically nonlinear reduced-order models with nonlinear normal modes, AIAA J. 53 (11) (2015) 3273–3285.
[16] M. McEwan, J.R. Wright, J.E. Cooper, A.Y.T. Leung, A combined modal/finite element analysis technique for the dynamic response of a non-linear beam to harmonic excitation, J. Sound Vib. 243 (4) (2001) 601–624.
[17] M. McEwan, J. Wright, J. Cooper, A. Leung, A finite element/modal technique for nonlinear plate and stiffened panel response prediction, in: 19th AIAA Applied Aerodynamics Conference, 2001, p. 1595.
[18] J.J. Hollkamp, R.W. Gordon, S.M. Spottswood, Nonlinear modal models for sonic fatigue response prediction: a comparison of methods, J. Sound Vib. 284 (3–5) (2005) 1145–1163.
[19] J.J. Hollkamp, R.W. Gordon, Reduced-order models for nonlinear response prediction: Implicit condensation and expansion, J. Sound Vib. 318 (4–5) (2008) 1139–1153.
[20] G. Haller, S. Ponsioen, Nonlinear normal modes and spectral submanifolds: existence, uniqueness and use in model reduction, Nonlinear Dynam. 86 (3) (2016) 1493–1534.
[21] R. Szalai, D. Ehrhardt, G. Haller, Nonlinear model identification and spectral submanifolds for multi-degree-of-freedom mechanical vibrations, Proc. R. Soc. A 473 (2202) (2017) 20160759.
[22] J.B. Rutzmoser, D.J. Rixen, P. Tiso, S. Jain, Generalization of quadratic manifolds for reduced order modeling of nonlinear structural dynamics, Comput. Struct. 192 (2017) 196–209.
[23] C. Touzé, A. Vizzaccaro, O. Thomas, Model order reduction methods for geometrically nonlinear structures: a review of nonlinear techniques, Nonlinear Dynam. 105 (2) (2021) 1141–1190.
[24] Y. Shen, N. Béreux, A. Frangi, C. Touzé, Reduced order models for geometrically nonlinear structures: Assessment of implicit condensation in comparison with invariant manifold approach, Eur. J. Mech. A Solids 86 (2021) 104165.
[25] E. Nicolaidou, V.R. Melanthuru, T.L. Hill, S.A. Neild, Accounting for quasi-static coupling in nonlinear dynamic reduced-order models, J. Comput. Nonlinear Dyn. 15 (7) (2020).
[26] V. Denis, M. Jossic, C. Giraud-Audine, B. Chomette, A. Renault, O. Thomas, Identification of nonlinear modes using phase-locked-loop experimental continuation and normal form, Mech. Syst. Signal Process. 106 (2018) 430–452.
[27] C.I. Van Damme, M.S. Allen, J.J. Hollkamp, Updating geometrically nonlinear reduced-order models using nonlinear modes and harmonic balance, AIAA J. 58 (8) (2020) 3553–3568.
[28] K. Park, M.S. Allen, Tuning of finite element model parameters to match nonlinear reduced order models, in: Nonlinear Structures & Systems, Vol. 1, Springer, 2021, pp. 113–116.
[29] C.E. Rasmussen, Advanced lectures on machine learning, Gaussian Process. Mach. Learn. (2004) 63–71.
[30] E. Schulz, M. Speekenbrink, A. Krause, A tutorial on Gaussian process regression: Modelling, exploring, and exploiting functions, J. Math. Psych. 85 (2018) 1–16.
[31] J.S. Hesthaven, S. Ubbiali, Non-intrusive reduced order modeling of nonlinear problems using neural networks, J. Comput. Phys. 363 (2018) 55–78.
[32] M. Guo, J.S. Hesthaven, Reduced order modeling for nonlinear structural analysis using Gaussian process regression, Comput. Methods Appl. Mech. Engrg. 341 (2018) 807–826.
[33] M. Guo, J.S. Hesthaven, Data-driven reduced order modeling for time-dependent problems, Comput. Methods Appl. Mech. Engrg. 345 (2019) 75–99.
[34] W. Chen, Q. Wang, J.S. Hesthaven, C. Zhang, Physics-informed machine learning for reduced-order modeling of nonlinear problems, J. Comput. Phys. 446 (2021) 110666.
[35] K. Hasegawa, K. Fukami, T. Murata, K. Fukagata, Machine-learning-based reduced-order modeling for unsteady flows around bluff bodies of various shapes, Theor. Comput. Fluid Dyn. 34 (4) (2020) 367–383.
[36] Z. Ma, W. Pan, Data-driven nonintrusive reduced order modeling for dynamical systems with moving boundaries using Gaussian process regression, Comput. Methods Appl. Mech. Engrg. 373 (2021) 113495.
[37] C. Touzé, M. Vidrascu, D. Chapelle, Direct finite element computation of non-linear modal coupling coefficients for reduced-order shell models, Comput. Mech. 54 (2) (2014) 567–580.
[38] A. Givois, A. Grolet, O. Thomas, J.-F. Deü, On the frequency response computation of geometrically nonlinear flat structures using reduced-order finite element models, Nonlinear Dynam. 97 (2) (2019) 1747–1781.
[39] C.K. Williams, C.E. Rasmussen, Gaussian Processes for Machine Learning, Vol. 2, MIT press Cambridge, MA, 2006.
[40] G. Kerschen, M. Peeters, J.-C. Golinval, A.F. Vakakis, Nonlinear normal modes, Part I: A useful framework for the structural dynamicist, Mech. Syst. Signal Process. 23 (1) (2009) 170–194.
[41] T. Detroux, L. Renson, L. Masset, G. Kerschen, The harmonic balance method for bifurcation analysis of large-scale nonlinear mechanical systems, Comput. Methods Appl. Mech. Engrg. 296 (2015) 18–38.
[42] R. Gordon, J. Hollkamp, S. Spottswood, Nonlinear response of a clamped-clamped beam to random base excitation, in: Proceedings of the Eighth International Conference on Recent Advances in Structural Dynamics, The Inst. of Sound and Vibration Southampton, England, UK, 2003.
[43] K. Park, M.S. Allen, Quasi-static modal analysis for reduced order modeling of geometrically nonlinear structures, J. Sound Vib. 502 (2021) 116076.
[44] C. Van Damme, M. Allen, J. Hollkamp, Evaluating reduced order models of curved beams for random response prediction using static equilibrium paths, J. Sound Vib. 468 (2020) 115018.